Journal of Physics: Conference Series

PAPER • **OPEN ACCESS**

Hierarchical structure and antibacterial activity of olive oil based $MZFe_2O_4$ ferrofluids

To cite this article: Defi Yuliantika *et al* 2020 *J. Phys.: Conf. Ser.* **1436** 012145

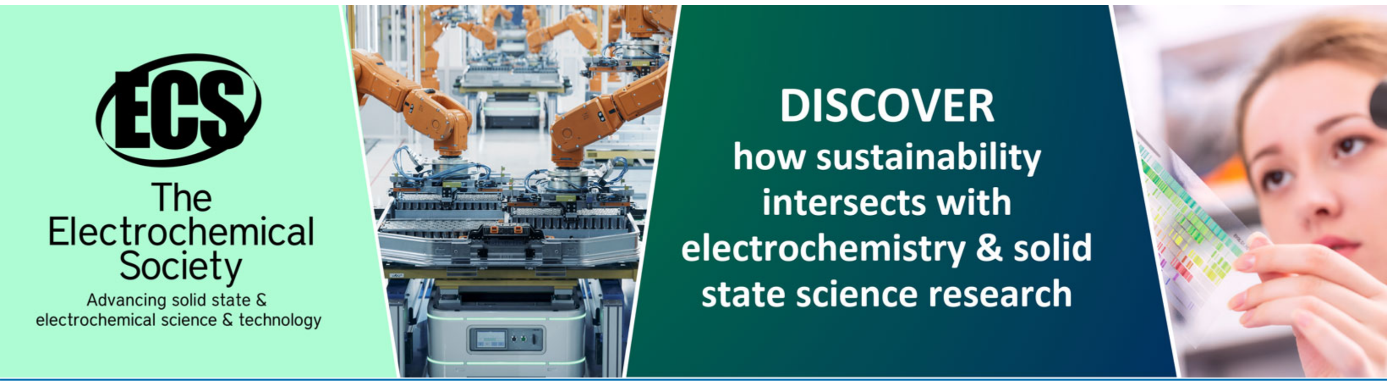

Hierarchical structure and antibacterial activity of olive oil based $MZFe_2O_4$ ferrofluids

Defi Yuliantika[1], Ahmad Taufiq[1], Edy Giri Rahman Putra[2]

[1]Department of Physics, Faculty of Mathematics and Natural Sciences, Universitas Negeri Malang, Indonesia
[2]Polytechnic Institute of Nuclear Technology, National Nuclear Enegy Agency (BATAN), Jl. Babarsari PO Box 6101 YKBP Telp(0274)484085, Fax.(0274)489715 Yogyakarta, Indonesia 55281

Abstract. $MZFe_2O_4$ (Z = Zn; M = Mn) ferrofluids based on olive oil as liquid carrier was successfully prepared by coprecipitation route. The stability of the $MZFe_2O_4$ ferrofluids was maintained by using oleic acid as surfactant agent. Their morphology, crystal structure, fractal structure, and optical behaviours were investigated by means of SEM, XRD, SAXS, and UV-Vis spectroscopy. Furthermore, the potency as antibacterial agent of the $MZFe_2O_4$ ferrofluids was explored by dilution method. The analysis for the XRD data presented that the $MZFe_2O_4$ particles as fillers constructed in nanometric scale with cubic spinel structure. The SEM images of the $MZFe_2O_4$ powders tended to agglomerate with spherical shape. Moreover, the $MZFe_2O_4$ ferrofluids constructed complex structure with aggregated fractal originated by interaction of internal force of magnetic particles. Theoretically, such phenomenon is predicted as the effect of filler, surfactant, and liquid carrier in the ferrofluids. Interestingly, the $MZFe_2O_4$ ferrofluids demonstrated superior performance as antibacterial agent than those of $MZFe_2O_4$ nanopowders. Technically, the superior performance of the ferrofluids is believed from its significant enhancing inhibition zone diameter as the effect of olive oil as an appropriate carrier.

1. Introduction

Study on nanostructure is one of priorities in nanomaterials research field. This case is because the structure of particular material in bulk condition is different from nanometric condition. Some studies showed that the structural characteristics of nanomaterials influenced other properties such as magnetization [1], mechanics [2], optics [3], electrics [4], and biomedicines [5]. One of nanomaterials that are massively studied is ferrite-based ferrofluids. In general, the ferrofluids exhibit excellent characteristics because they can be confined, deformed, and controlled by an external magnetic field [6]. Therefore, in recent years, application of the ferrofluids has increased significantly in various areas, especially for nanomedical artificial intelligence [7], [8], [9]. Theoretically, there are three main components of ferrofluids, i.e. filler, surfactant, and dispersing agent. In general, ferrofluid fillers are magnetic nanoparticles significantly contributing to determine the physical properties of ferrofluids. One of the fillers often researched is Fe_3O_4 since it has chemical stability, photocatalytic properties, and good response to external magnetic field. The previous studies showed that the substitution of Fe_3O_4 with Mn atom significantly improved photocatalytic activity and magnetic saturation [10], [11] in medical sensor application and drug delivery technology. Meanwhile, the substitution of the non-toxic Zn atom could improve the biocompatibility of material [12]. Therefore, this work substituted metal atoms (Mn and Zn) to form $MZFe_2O_4$ compound to enhance its application performance. So far, magnetic nanoparticles dispersed in liquid media tend to aggregate due to van der Waals force. Hence, a repulsive force is needed to balance the interaction between particles and to prevent aggregation.

One of the strategic steps is modifying surfactant using oleic acid. As surfactant, oleic acid can coat magnetic particles and create minimum distance between particles by steric repulsive force [13]. Besides, oleic acid also can be a linker between filler and appropriate dispersing medium like olive oil. In general, olive oil has some advantages such as anti-inflammatory, anti-bacterial, biocompatibility, and good health effect that supports ferrofluid potential in the biomedical field. For further benefit of application, a hierarchical structure of ferrofluids is essential to be investigated because it influences physical characteristics such as magnetization, optic, and stability [14], [15]. Principally, the nanostructure, including aggregation structure is strongly influenced by particle size and characteristics of fluids [16]. In other words, the aggregation structure between magnetic particles in the form of powders is different from ferrofluids. In general, the structural characterization is carried out by using a non-destructive method of X-Ray diffraction to identify structure, crystal parameter, and particle size. However, this method is limited to the characteristics of the powder sample type. Electron microscope method is one of the alternatives since it results in real image data in the form of particle size and morphology of material. However, both characterizations have weakness in characterizing the samples in the form of fluids. Furthermore, the other weaknesses are characterization limited in some sample areas, the difficulty in determining particle size in data containing stacked particles, and complicated sample preparation [17]. Therefore, one of very promising characterization methods in examining particle behavior in ferrofluids system is by using small-angle X-ray scattering (SAXS). As nondestructive test and easy in preparation sample, SAXS method informs the particle size, size distribution, and structural hierarchy of various samples. SAXS is an indirect method since the characteristics of ferrofluid structure are obtained from scattering statistic data. Hence, in this work, we investigated the hierarchical structure of the $MZFe_2O_4$ ferrofluids in olive oil medium using SAXS method. Moreover, the other characteristics related to functional groups, optical properties, and anti-bacterial activity of the $MZFe_2O_4$ ferrofluids were also investigated.

2. Methodology

Magnetite was extracted from iron sand of Sine Beach, Indonesia by using magnetic separation method. Extraction was undertaken many times to reduce impurity compounds through washing process by distilled water, then following by drying process under sunlight. After the iron sand was dry, the samples were sieved to result in fine sand. Subsequently, the magnetite were separated from using a permanent magnet. A twenty grams of iron sand which had been separated was dissolved in 58 ml of HCl (Molarity = 12 M, 99.9%) and stirred in magnetic stirrer for 20 minutes at room temperature. The iron sand was dissolved in hydrochloric acid to form a chemical reaction shown by Equation (1).

$$Fe_3O_{4(s)} + 8\ HCl_{(l)} \rightarrow 2\ FeCl_{3(l)} + FeCl_{2(l)} + 4\ H_2O_{(l)} \tag{1}$$

The formed solution was filtered using filter paper. 15 ml of the brown liquid passing the filtering was taken to be reacted with metal chloride ($MnCl_2$ and $ZnCl_2$) with a certain concentration and then dropped wisely with 20 mL of NH_4OH (Molarity = 6.5 M, 99.9%) into hotplate magnetic stirrer with a rotation speed of 750 rpm at room temperature for 30 minutes. The reaction mechanism of ferrite forming is presented in the following reaction as shown as Equation (2).

$$2\ FeCl_3 + FeCl_2 + x\ (MZ)Cl_2 + 8\ NH_4OH \rightarrow (MZ)Fe_2O_4 + 8\ NH_4Cl + 4H_2O \tag{2}$$

After that process, the result was washed repeatedly using distilled water until pH = 7. Finally, one gram of the filtering result was taken to be mixed with oleic acid and dispersed into olive oil with a ratio of 1:2 mL. Meanwhile, ferrite nanoparticles in powders were obtained by calcination at a temperature of 100 ºC during 60 minutes and then finely grinded. Characterizations of crystal structure, fractal structure, chemical compound as functional groups, optical properties were conducted by means of XRD, SAXS, FTIR, and UV-Vis. Meanwhile, the antibacterial activity of the $MZFe_2O_4$ ferrofluids was characterized using liquid dilution method for *E.coli* gram-negative bacteria and *S.Aureus* gram-positive bacteria.

3. Results and Discussion

Functional groups of the $MZFe_2O_4$ ferrofluids were characterized using FT-IR spectroscopy in the form of a graph of the relationship between wavenumber and transmittance value. The transmittance peak showed vibration of the atom bond. The $MZFe_2O_4$ ferrofluids consisted of metal bond indicated by the wavenumber of 400- 1000 cm^{-1} [18] and organic bond by olive oil compound and oleic acid surfactant. The graph of FT-IR in forming the $MZFe_2O_4$ ferrofluids based on olive oil is presented in Figure 1.

The transmittance peaks of the metal can be seen in the wavenumber of 580, 448, and 994 cm^{-1} as the vibration of tetrahedral M-O and octahedral M-O bonds [19]. This case indicated the forming of a spinel structure [20]. The organic compound can be seen in the higher wavenumber. The higher the ionic coordination (bond length), the vibration mode would be weaker due to the stretching force and compression of ionic bonds [21], [22] and caused organic bond migrate to the higher wavenumber. In detail, the vibrations of the $MZFe_2O_4$ ferrofluids observed in the FTIR spectra is tabulated in Table 1.

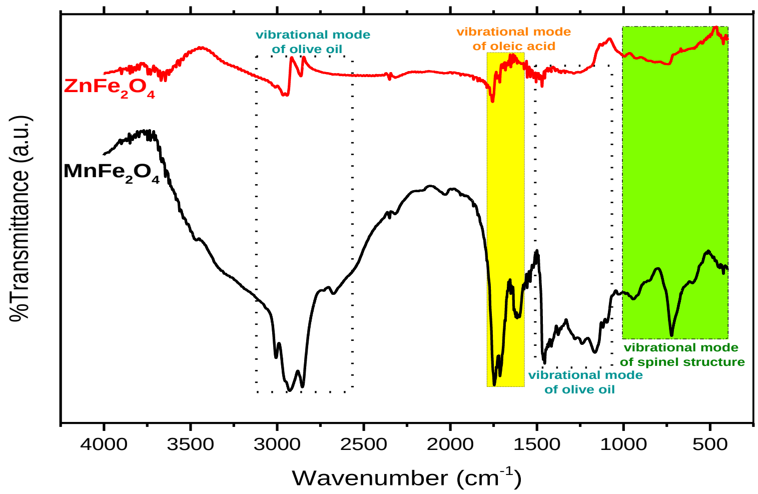

Figure 1. Infra-red spectra of the $MZFe_2O_4$ ferrofluids

Table 1. Functional groups of the $MZFe_2O_4$ ferrofluids

Compound	Vibration Peak	Note	References
Spinel structure	448 cm^{-1}	Vibration of tetrahedral M-O	[23]
	580 cm^{-1}	Vibration of octahedral coordinate M-O	[23,24]
	944 cm^{-1}	Vibration of Spinel	[24]
Olive oil	723 cm^{-1}	Vibration of δCH_2 – the bond of aliphatic compound	[25]
	1162 cm^{-1}	Vibration of C=O and $-CH_2$ ester bonds	[25]
	1460 cm^{-1}	Vibration of δCH_2 bond	[26]
	1754 cm^{-1}	Vibration of νC=O carbonyl triacylglycerols	[26]
	2846 cm^{-1}	νCH2 – the vibration of hydroperoxide fat acid	[27]
	2925 cm^{-1}	CH3 – the vibration of hydroperoxide fat acid	[28]

	3007 cm^{-1}	Unsaturated vibration of C-H, νC-H	[26]
Oleic acid	1621- 1710 cm^{-1}	Absorption peak of carboxyl peak	[29,30]

Structural characteristics of the crystal phase, lattice parameters, and particle size of the $MZFe_2O_4$ nanoparticles in powders were analyzed through X-ray diffraction using radiation source of Cu-Kα with the wavelength of 1.5406 Å. Figure 2 shows the X-ray diffraction patterns of the $MZ.Fe_2O_4$ nanoparticles in powders. The diffraction peaks detected indicated spinel phase with *Fd-3m* space group with *hkl* planes of (220), (311), (400), (422), (511), (440), (531), and (442) [31]. The data were analyzed using AMCSD 0000945 data model through Rietveld analysis. The analysis results informed that the crystal structure of the $MZFe_2O_4$ nanoparticles was mixed-spinel structure since the metal ions were distributed in tetrahedral and octahedral positions where the lattice parameters as the calculation results is presented in Table 2 [32], [33].

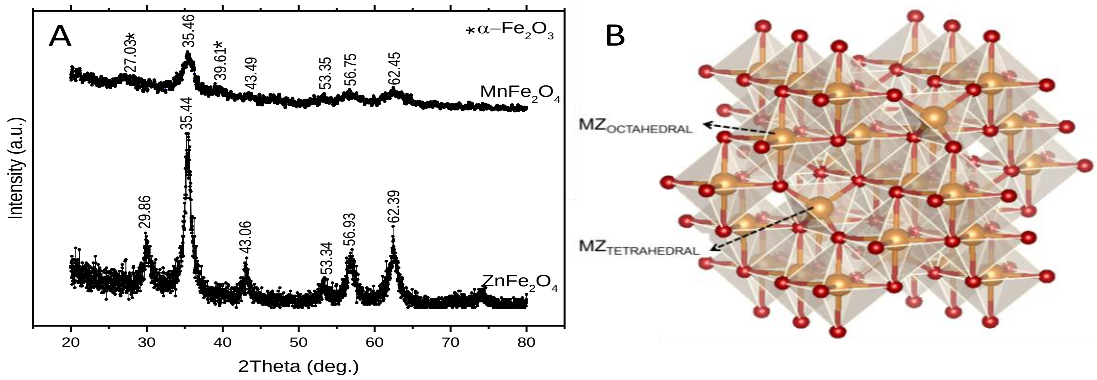

Figure 2. (A) X-ray diffraction patterns and (B) mixed-spinel structure of the $MZFe_2O_4$ nanoparticles

The analysis results showed that the diffraction peaks of the $ZnFe_2O_4$ nanoparticles appearing at the value of 2 Theta was in accordance with the data model. Interestingly, there were other peaks at 2 Theta namely 27.8° and 39.61° which indicated that there was another phase, namely α-Fe_2O_3 [34], [35]. The α-Fe_2O_3 phase in $MnFe_2O_4$ sample was caused by chemical instability due to excessive iron ions in $MnFe_2O_4$ phase so that the iron ions unbound with Mn would be bound with free oxygen resulting in Fe_2O_3 [36]. The calculation results of particle size using Scherrer method showed that the $MnFe_2O_4$ had smaller particles size than $ZnFe_2O_4$ because Mn^{2+} had smaller ionic radius (66 pm) than Zn^{2+} (74 pm). Crystal structure and particle size of the samples are presented in Table 2.

Spinel structure of $MZFe_2O_4$ nanoparticles in this research confirms the study on $MnFe_2O_4$ and $ZnFe_2O_4$ conducted by Silva *et al.* and Nikolic *et al.*, respectively. The forming of mixed-spinel structure coordination in the ferrite phase was reported that it could improve magnetism, electricity, and gas sensor capability [37], [38]. Above and beyond, coprecipitation synthesis method using iron sand successfully formed $MZFe_2O_4$ particles with a particle size of ± 10 nm smaller than the magnetic particles prepared by using combustion and gel calcination methods using commercial chemical material. The lower the magnetic particle size approaching the single domain of ± 10 nm, the particles could behave superparamagnetic character [39].

Table 2. Crystal structure and particle size of $MZFe_2O_4$ nanoparticles

Sample	Spinel Structure	2-theta of (311) peak	Lattice Parameters (Å)	Particle Size (nm)
$MnFe_2O_4$	$\left[Mn_{0.5}^{2+}Fe_{0.5}^{3+}\right]_A\left[Mn_{0.5}^{2+}Fe_{0.5}^{2+}Fe_1^{3+}\right]_B O_4$	35.4674°	8.3947	6.24
$ZnFe_2O_4$	$\left[Zn_{0.5}^{2+}Fe_{0.5}^{3+}\right]_A\left[Zn_{0.5}^{2+}Fe_{0.5}^{2+}Fe_1^{3+}\right]_B O_4$	35.4445°	8.4148	9.49

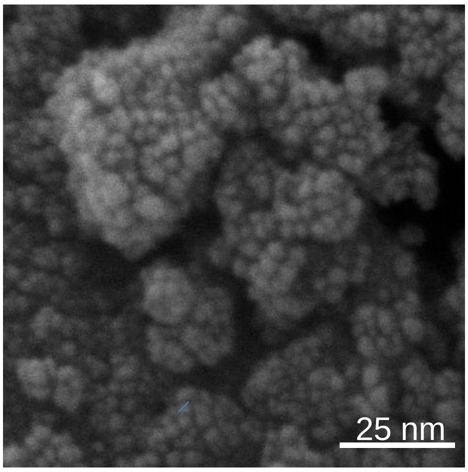

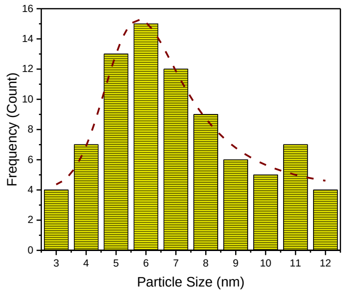

Element	Wt%	At%
CK	07.77	21.64
OK	15.38	32.17
MnK	14.92	09.09
FeK	61.93	37.10
Matrix	Correction	ZAF

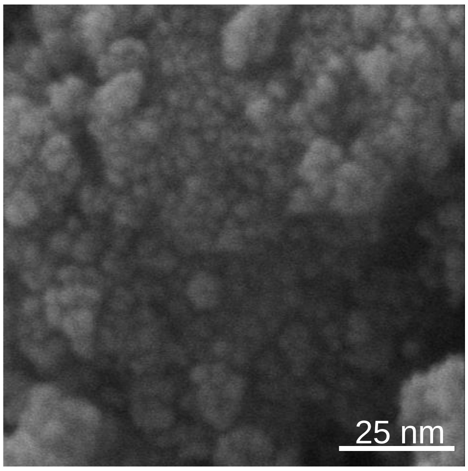

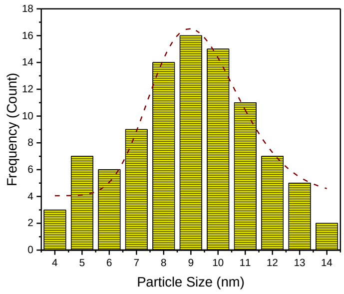

Element	Wt%	At%
CK	14.71	34.61
OK	18.52	32.72
FeK	51.46	26.05
ZnK	15.31	06.62
Matrix	Correction	ZAF

Figure 3. SEM-EDX profiles of $MZFe_2O_4$ nanoparticles

Characterization of morphology, particles size distribution, and content of elements in $MZFe_2O_4$ nanoparticles was carried out using SEM-EDAX. The SEM images as shown in Figure 3 present that the $MZFe_2O_4$ particles had a spherical form. Quantitative analysis resulted in histogram informs the particle size distribution of the $MZFe_2O_4$. The histograms indicate that the nanoparticles had lognormal distribution pattern where the $ZnFe_2O_4$ had mean particle size of 9.24 ± 0.19 nm and polydispersity index of 0.20, while the $MnFe_2O_4$ had mean particle size of 6.15 ± 0.13 nm and polydispersity index of 0.21.

The elemental content of the $MZFe_2O_4$ nanoparticles was analyzed to identify the ratio of elements as the results of calculation by synthesis. In $Mn.Fe_2O_4$ samples, the synthesis resulted in Mn:Fe of 0.6:2.4 where the notation of compound formed could be written with $Mn_{0.6}Fe_{2.4}O_4$, while in $ZnFe_2O_4$ the synthesis resulted in the ratio of Zn:Fe namely 0.7:2.3 and thus obtaining $Zn_{0.7}Fe_{2.3}O_4$. The synthesis results were different from the calculation results because of the use of iron sand as the natural raw material.

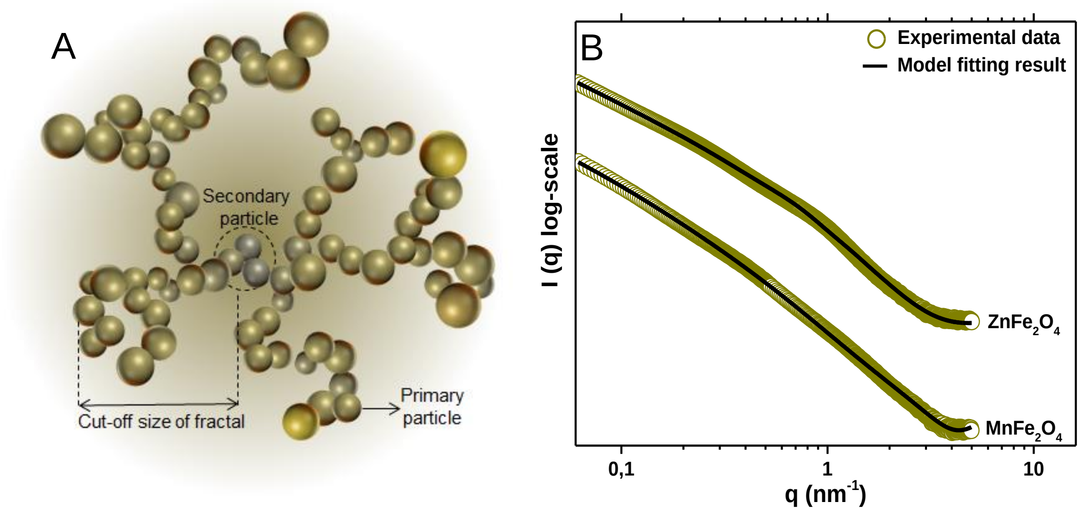

Figure 4. Illustration of hierarchical structure (A) and scattering profiles (B) of the $MZFe_2O_4$ ferrofluids

The stability of ferrofluid phase was resulted by the balance of repulsive force provided by a surfactant to van der Waals force produced by the interaction between particles resulting in magnetic particles. When external magnetic field acts on ferrofluids, the direction of magnetic moments follows the external magnetic field resulting an aggregation of the magnetic particles like a chain in which the dipole was oriented in the configuration of head to tail. However, another work showed that the chain aggregate was formed although without external magnetic field [40]. Therefore, in this work, $MZFe_2O_4$ ferrofluids were characterized using by SAXS to examine their particle configuration without external magnetic field. Figure 4 presents SAXS profiles plotted in the graph of the relationship between momentum transfer (q) and scattering intensity $I(q)$. SAXS analysis was carried out to identify the distribution of particle size in the range of q ($q=2\pi/d$), where d is the particle size of the sample. The scattering intensity of the samples informed the form factor $P(q, R)$; structural factor $S(q, R)$; and size distribution $D(R)$ written in Equation 3.

$$I_{np}(q) = C_{np}\int_0^\infty P_{np}(q,R)S_{np}(q,R)R^6 D_{np}(R)dR \tag{3}$$

where C_{np} is the factor scale. Analysis of form factor with spherical model and lognormal size distribution was applied following SEM analysis results. Meanwhile, the structural factor was analyzed using mass fractal model (*Exp cut off*). Mathematically, the form factor, size distribution, and structural factor in SAXS analysis are written in Equation 4-6.

$$P_{np}(q,R) = 9\left[\frac{\sin(qR) - qR\cos(qR)}{(qR)^3}\right]^2 \tag{4}$$

$$D_{np}(R) = \frac{N}{\sqrt{2\pi\sigma^2}R}\exp\left[\left[\ln(R/R_o)\right]^2/2\sigma^2\right] \tag{5}$$

$$S_{frac}(q,r_0) = 1 + \frac{D}{r_0^D}\int_0^\infty R^{(D-3)}h(r,\xi).\frac{\sin(qr)}{qr}.r^2dr \tag{6}$$

$D_{np}(R)$ represents the lognormal distribution; σ is the polydispersity index; R_o is the particle radius mean, N is the normalization factor; ξ is the cut-off length of fractal correlation; and D is the fractal dimension [6].

Table 3 provides information on SAXS analysis results. The $MZFe_2O_4$ nanoparticles had high polydispersity index with primary particle size in the dimension of < 5 nm. The tendency of primary particle aggregation caused the forming of higher size dimension reaching 10 nm known as secondary particles. Subsequently, the secondary particles correlated each other to form a chain-like aggregate with the fractal cut-off correlation length of 100 nm. The aggregate structure was in the form of surface fractal with dimension of approximately 2. The structural illustration by SAXS is shown in Figure 4A. The secondary particle size attained through SAXS approached that of SAXS and XRD analyses.

This case showed that the things examined in XRD and SEM were contributed by secondary particles. Meanwhile, in ferrofluids, the dispersed particles in the fluids indicated monomer characteristic with particle size approaching single domain.

Table 3. Particle sizes, fractal dimension, and distribution of the $MZFe_2O_4$ ferrofluids

	$MnFe_2O_4$	**$ZnFe_2O_4$**
Primary particle size (μ) nm	4.82	4.04
Secondary particle size (r_0) nm	7.06	9.99
Fractal cut-off length (ξ) nm	85.0	92.3
Fractal dimension (D)	1.78	1.90

The optical properties of the $MZFe_2O_4$ ferrofluids were characterized by using UV-Vis spectrophotometer. The wavelength used in the range of 200 to 800 nm is presented in Figure 5. In Figure 5, there is an absorbance peak at the wavelength of around 500 nm as the characteristic of absorbance of iron metal element where the $MnFe_2O_4$ samples had a bit higher absorbance value than $ZnFe_2O_4$. Hence, the increasing absorptivity of material caused the increase in absorbance intensity based on Lambert beer law in Equation 7,

$$Abs = -\log(I / I_0) = \varepsilon dc \tag{7}$$

Where I is the light intensity transmitted by the material, I_0 is the incident light intensity, ε is the absorptivity coefficient, d is the path-length, and c is the liquid concentration. By analysis using Tauc equation, the bandgap energy value of each sample could be found. The bandgap energy values were calculated by extrapolating the value of $\alpha = 0$ in the graph of linear relationship between $h\upsilon$ and $(\alpha h\upsilon)^2$, which resulted in bandgap energy value of $MnFe_2O_4$ ferrofluids and $ZnFe_2O_4$ ferrofluids of 2.28 eV and 2.26 eV, respectively. Mathematically, the bandgap energy value was inversely related to particle size due to quantum size effect that caused conduction and valence bands shifted to the space boundary between charges [41].

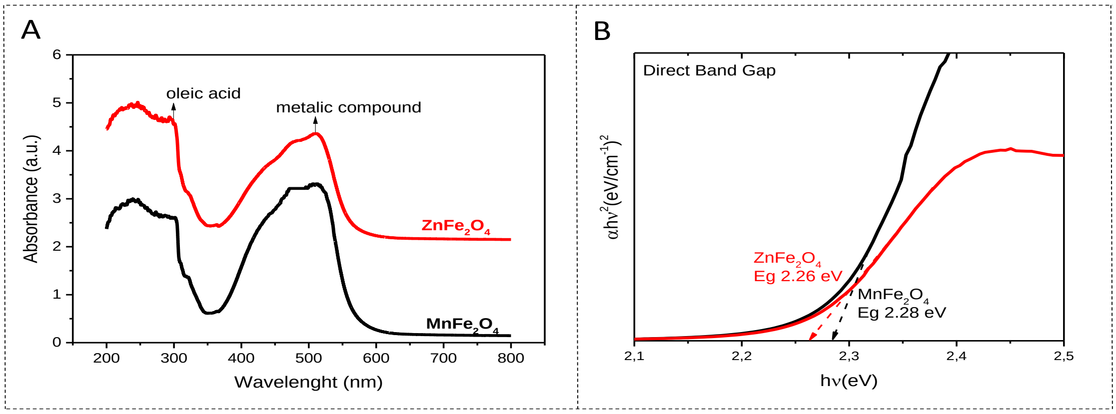

Figure 5. UV-Vis spectrum (A) and Tauc plot (B) of the $MZFe_2O_4$ ferrofluids

Besides metal compound, there was an absorption spectrum of olive oil compound in the wavelength of 290 nm appearing in olive oil-based $MZFe_2O_4$ ferrofluids. This case is in line with the previous research conducted by Fuentes *et al*. that characterized the olive oil absorption appearing in the wavelength of 300 nm [42]

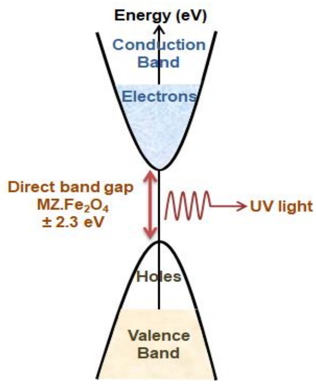

Figure 6. Direct bandgap structure of the $MZFe_2O_4$ ferrofluids

In this work, the dilution method was used to examine the antibacterial activity of $MZFe_2O_4$ in ferrofluids in nanopowders. The antibacterial activity was determined based on the ratio of the number of live bacterial colony after being treated by samples. Furthermore, the ability of the samples and conventional drug namely erythromycin to kill bacteria was also studied. The fewer the live bacteria, the better the anti-bacterial ability [43] proven by the percentage of the dead bacteria. Erythromycin is an antibiotic commonly used to kill bacteria since it has a better anti-bacteria ability than Sthreptomicyn and Penisilin [44].

The dilution characterization results shown in Figure 7 and 8 indicate that the $ZnFe_2O_4$ ferrofluids could kill the *E.Coli* bacteria well even better than erythromycin antibiotic. It can be seen that the number of *E. coli* bacteria colony after treated by using the $ZnFe_2O_4$ ferrofluids was fewer than erythromycin with bacteria mortality of 99.32% while the $MnFe_2O_4$ ferrofluids resulted in mortality of 71.81%. Meanwhile, in nanopowders, the antibacterial activity was unseen. The tendency of antibacterial activity was different from *B. subtilis* bacteria which showed that the $MZFe_2O_4$ nanopowders was less reactive to gram-positive bacteria.

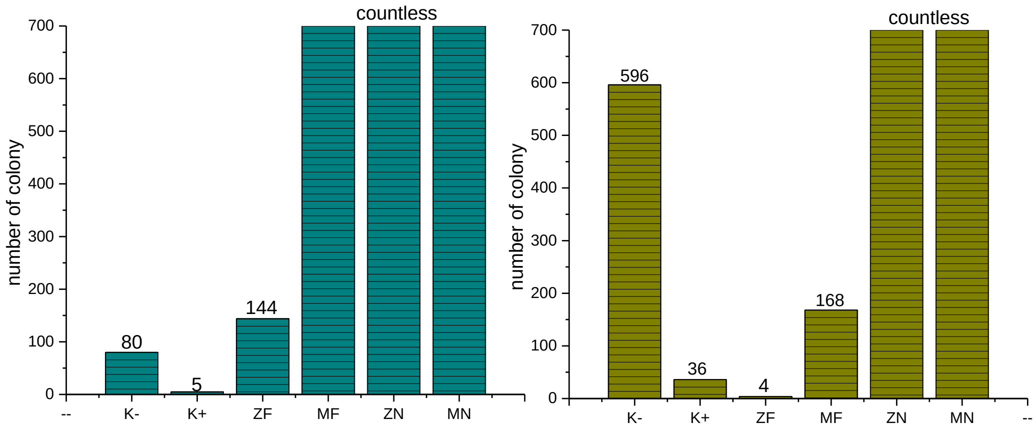

Figure 7. Survival colony count of bacterial without treatment (K-), Erythromycin drug (K+) of the $ZnFe_2O_4$ ferrofluids (ZF), the $MnFe_2O_4$ ferrofluids (MF), $ZnFe_2O_4$ nanopowders (ZN) and the $MnFe_2O_4$ nanopowders (MN) by agar dilution methods.

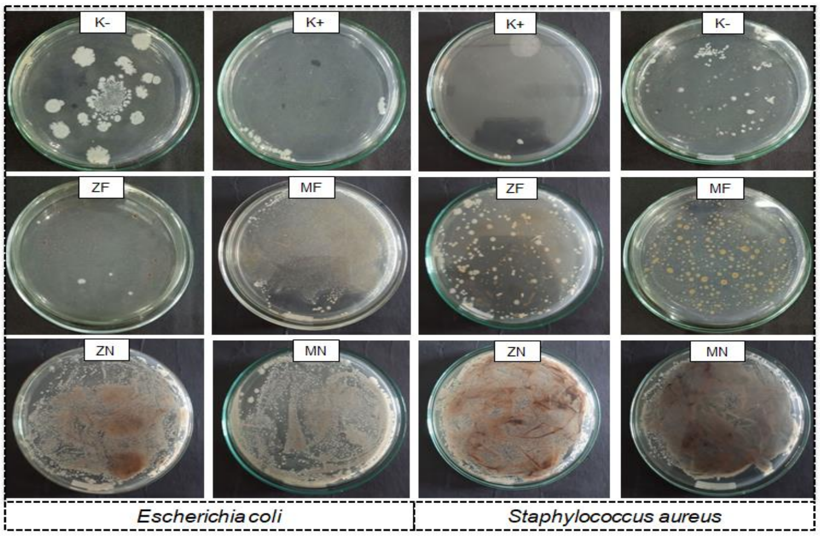

Figure 8. Photograph of the bacterial colony without treatment (K-), Erythromycin drug (K+). $ZnFe_2O_4$ ferrofluids (ZF), $MnFe_2O_4$ ferrofluids (MF), $ZnFe_2O_4$ nanopowder (ZN) and $MnFe_2O_4$ nanopowder (MN) by agar dilution methods.

One of the good antibacterial activities in ferrofluids is resulted by interaction between cation and anion compounds contained in the materials. The presence of Zn^{2+} ion can stop the process of cell division when it reacts with enzyme and bacterial protein which then initializes the damage of cell wall and cytoplasm [45]. In addition, the use of olive oil containing dialdehyde compound is reactive to bacterial cell membrane so that the bacterial growth is inhibited [46]. The process of bacterial killing depends on how the material can penetrate cell membrane and diffuse into cell inner, deactivate enzyme, inhibit the protease forming, denature protein, and then the bacterial cell will die where this case can be done by the $MZFe_2O_4$ ferrofluids. The chain structure of the $ZnFe_2O_4$ ferrofluids that had longer fractal cut-off size than that of the $MnFe_2O_4$ ferrofluids helped the material to penetrate and diffuse into cell membrane [47]. This case indicated that antibacterial properties of samples were influenced by fractal structure of ferrofluids.

4. Conclusion

Synthesis of the olive oil-based $MZFe_2O_4$ ferrofluids by using coprecipitation method resulted in nanoparticles with the particle size of <10 nm and mixed spinel structure. The functional groups of the $MZFe_2O_4$ as fillers, oleic acid as surfactant, and olive oil as dispersing agent were detected on various wavenumbers. In the ferrofluids, the particles formed surface fractal structure with fractal dimension value of 2. The $MZFe_2O_4$ ferrofluids had the primary particle size of 5 nm aggregated to form 10 nm secondary particles. The interaction between particles, dispersant, and surfactant in the ferrofluids caused particles correlated to form chain-like structure with 100 nm cut-off. The optical properties regarding absorbance and bandgap values showed that the $MZFe_2O_4$ ferrofluids had absorbance values in the wavelength of 500 nm and the direct bandgap in the range of 2.2 eV. The difference in bandgap energy value in the $MZFe_2O_4$ nanoparticles was influenced by the particle size. Furthermore, the antibacterial activity to *E.Coli* and *S.Aureus* indicated that the $ZnFe_2O_4$ ferrofluids were excellent in killing bacteria colony proven by the percentage of cell mortality reaching 99.32%.

Acknowledgments

This work was supported by Universitas Negeri Malang through PNBP research grant.

References

[1] Ahmad T, Triwikantoro T, Pratapa S and Darminto D 2009 Sintesis Partikel Nano $Fe_{3-x}Mn_xO_4$ Berbasis Pasir Besi dan Karakterisasi Struktur serta Kemagnetannya *Jurnal Nanosains & Nanoteknologi* **1** 67–73
[2] Baghban A, Sasanipour J, Pourfayaz F, Ahmadi M H, Kasaeian A, Chamkha A J, Oztop H F and Chau K 2019 Towards experimental and modeling study of heat transfer performance of water- SiO_2 nanofluid in quadrangular cross-section channels *Engineering Applications of Computational Fluid Mechanics* **13** 453–69
[3] Bahrani S, Hashemi S A, Mousavi S M and Azhdari R 2019 Zinc-based metal–organic frameworks as nontoxic and biodegradable platforms for biomedical applications: review study *Drug Metabolism Reviews* **51** 356–77
[4] Bonini M, Fratini E and Baglioni P 2007 SAXS study of chain-like structures formed by magnetic nanoparticles *Materials Science and Engineering: C* **27** 1377–81
[5] Borchert H, Shevchenko E V, Robert A, Mekis I, Kornowski A, Grübel G and Weller H 2005 Determination of Nanocrystal Sizes: A Comparison of TEM, SAXS, and XRD Studies of Highly Monodisperse $CoPt_3$ Particles *Langmuir* **21** 1931–6
[6] Damayanti E, Julendra H, Sofyan A and Hayati S N 2014 Bile Salt and Acid Tolerant of Lactic Acid Bacteria Isolated from Proventriculus of Broiler Chicken *Media Peternakan* **37** 80
[7] De la Mata P, Dominguez-Vidal A, Bosque-Sendra J M, Ruiz-Medina A, Cuadros-Rodríguez L and Ayora-Cañada M J 2012 Olive oil assessment in edible oil blends by means of ATR-FTIR and chemometrics *Food Control* **23** 449–55
[8] Estrada S O, Huerta-Aguilar C A, Pandiyan T, Corea M, Reyes-Domínguez I A and Tavizon G 2017 Tuning of the magnetic response in cobalt ferrite $Co_xFe_{3-x}O_4$ by varying the Fe^{2+} to Co^{2+} molar ratios: Rietveld refinement and DFT structural analysis *Journal of Alloys and Compounds* **695** 2706–16
[9] Fuentes E, Báez M E, Bravo M, Cid C and Labra F 2012 Determination of Total Phenolic Content in Olive Oil Samples by UV–visible Spectrometry and Multivariate Calibration *Food Analytical Methods* **5** 1311–9
[10] Fortes Brollo M E, Hernández Flores P, Gutiérrez L, Johansson C, Barber D F and Morales M del P 2018 Magnetic properties of nanoparticles as a function of their spatial distribution on liposomes and cells *Physical Chemistry Chemical Physics* **20** 17829–38

[11] Hakim A, Marliza T S, Abu Tahari N M, Wan Isahak R W N, Yusop R M, Mohamed Hisham W M and Yarmo A M 2016 Studies on CO $_2$ Adsorption and Desorption Properties from Various Types of Iron Oxides (FeO, Fe_2O_3 , and Fe_3O_4) *Industrial & Engineering Chemistry Research* **55** 7888–97
[12] Hakim L F, Portman J L, Casper M D and Weimer A W 2005 Aggregation behavior of nanoparticles in fluidized beds *Powder Technology* **160** 149–60
[13] Hamizi N A, Johan M R, Chowdhury Z Z, Wahab Y A, Al-Douri Y, Saat A M and Pivehzhani O A 2019 Raman spectroscopy and FTIR spectroscopy studies of Mn-doped CdSe QDs at different particles size *Optik* **179** 628–31
[14] Hatami S, Mohamadi Sani A and Yavarmanesh M 2016 Chemical composition and antibacterial activity of organic extra virgin olive oil from Iran *Nutrition & Food Science* **46** 388–95
[15] Hussen M K, Dejene F B and Tsega M 2019 Effect of pH on material properties of ZnAl2O4:Cr^{3+} nano particles prepared by sol–gel method *Journal of Materials Science: Materials in Electronics* **30** 10191–201
[16] Jaganathan S K, Mani M P, Ismail A F, Prabhakaran P and Nageswaran G 2019 Tailor-made multicomponent electrospun polyurethane nanofibrous composite scaffold comprising olive oil, honey, and propolis for bone tissue engineering *Polymer Composites* **40** 2039–50
[17] Kanagesan S, Aziz S, Hashim M, Ismail I, Tamilselvan S, Alitheen N, Swamy M and Purna Chandra Rao B 2016 Synthesis, Characterization and in Vitro Evaluation of Manganese Ferrite ($MnFe_2O_4$) Nanoparticles for Their Biocompatibility with Murine Breast Cancer Cells (4T1) *Molecules* **21** 312
[18] Khan J A, Jamal Y, Shahid A and Boulanger B O 2016 Esterification of acetic and oleic acids within the Amberlyst 15 packed catalytic column *Korean Journal of Chemical Engineering* **33** 582–6
[19] Koplovitz G, Leitus G, Ghosh S, Bloom B P, Yochelis S, Rotem D, Vischio F, Striccoli M, Fanizza E, Naaman R, Waldeck D H, Porath D and Paltiel Y 2019 Single Domain 10 nm Ferromagnetism Imprinted on Superparamagnetic Nanoparticles Using Chiral Molecules *Small* **15** 1804557
[20] Koutná N, Řehák P, Chen Z, Bartosik M, Fallmann M, Černý M, Zhang Z, Friák M, Šob M, Mayrhofer P H and Holec D 2019 Correlating structural and mechanical properties of AlN/TiN superlattice films *Scripta Materialia* **165** 159–63
[21] Liu S, Yao K, Fu L-H and Ma M-G 2016 Selective synthesis of Fe_3O_4, γ-Fe_2O_3 , and α-Fe_2O_3 using cellulose-based composites as precursors *RSC Advances* **6** 2135–40
[22] Long N V, Yang Y, Teranishi T, Thi C M, Cao Y and Nogami M 2015 Synthesis and magnetism of hierarchical iron oxide particles *Materials & Design* **86** 797–808
[23] Lysenko S N, Astaf'eva S A, Yakusheva D E and Balasoiu M 2019 Novel parameter predicting stability of magnetic fluids for possible application in nanocomposite preparation *Applied Surface Science* **463** 217–26
[24] Magioglou E, Frontistis Z, Vakros J, Manariotis I D and Mantzavinos D 2019 Activation of Persulfate by Biochars from Valorized Olive Stones for the Degradation of Sulfamethoxazole *Catalysts* **9** 419
[25] Moghadam R Z, Dizaji H R, Ehsani M H, Kameli P and Jannesari M 2019 Correlation study of structural, optical, and hydrophobicity properties of diamond-like carbon films prepared by an anode layer source *Materials Research Express* **6** 055601
[26] Mozaffari M, Shatooti S, Jafarzadeh M, Niyaifar M, Aftabi A, Mohammadpour H and Amiri S 2015 Synthesis of Zn^{2+} substituted maghemite nanoparticles and investigation of their structural and magnetic properties *Journal of Magnetism and Magnetic Materials* **382** 366–75
[27] Nawle A C, Humbe A V, Babrekar M K, Deshmukh S S and Jadhav K M 2017 Deposition, characterization, magnetic and optical properties of Zn doped $CuFe_2O_4$ thin films *Journal of Alloys and Compounds* **695** 1573–82

[28] Nikolic M V, Vasiljevic Z Z, Lukovic M D, Pavlovic V P, Krstic J B, Vujancevic J, Tadic N, Vlahovic B and Pavlovic V B 2019 Investigation of $ZnFe_2O_4$ spinel ferrite nanocrystalline screen-printed thick films for application in humidity sensing *International Journal of Applied Ceramic Technology* **16** 981–93
[29] Palanisamy K L, Devabharathi V and Sundaram N M 2013 The utility of magnetic iron oxide nanoparticles stabilized by carrier oils in removal of heavy metals from waste water *International Journal of Research in Applied, Natural and Social Sciences* **1** 15–22
[30] Paula F L de O 2019 SAXS Analysis of Magnetic Field Influence on Magnetic Nanoparticle Clusters *Condensed Matter* **4** 55
[31] Petrova E, Kotsikau D and Pankov V 2015 Structural characterization and magnetic properties of sol–gel derived $Zn_xFe_{3-x}O_4$ nanoparticles *Journal of Magnetism and Magnetic Materials* **378** 429–35
[32] Randall McClain K, Gould C A, Chakarawet K, Teat S J, Groshens T J, Long J R and Harvey B G 2018 High-temperature magnetic blocking and magneto-structural correlations in a series of dysprosium(III) metallocenium single-molecule magnets *Chemical Science* **9** 8492–503
[33] Ramezanizadeh M, Alhuyi Nazari M, Ahmadi M H, Lorenzini G and Pop I 2019 A review on the applications of intelligence methods in predicting thermal conductivity of nanofluids *Journal of Thermal Analysis and Calorimetry*
[34] Rathod V, Anupama A V, Kumar R V, Jali V M and Sahoo B 2017 Correlated vibrations of the tetrahedral and octahedral complexes and splitting of the absorption bands in FTIR spectra of Li-Zn ferrites *Vibrational Spectroscopy* **92** 267–72
[35] Reuter S, Weßkamp B, Büscher R, Fischer A, Barden B, Löer F and Buck V 2006 Correlation of structural properties of commercial DLC-coatings to their tribological performance in biomedical applications *Wear* **261** 419–25
[36] Sa'adah S M, Nawfa R and Purnomo A S 2016 Pengaruh Sabut Kelapa Sebagai Media Pertumbuhan Alternatif Jamur Tiram Putih (*Pleurotus ostreatus*) terhadap Aktivitas Antimikroba *Jurnal Sains dan Seni ITS* **5** C53–6
[37] Sharma S K 2019 *Nanohybrids in environmental & biomedical applications*
[38] Silva F G da, Depeyrot J, Campos A F C, Aquino R, Fiorani D and Peddis D 2019 Structural and Magnetic Properties of Spinel Ferrite Nanoparticles *Journal of Nanoscience and Nanotechnology* **19** 4888–902
[39] Sohail A, Fatima M, Ellahi R and Akram K B 2019 A videographic assessment of ferrofluid during magnetic drug targeting: An application of artificial intelligence in nanomedicine *Journal of Molecular Liquids* **285** 47–57
[40] Stuart B 2005 *Infrared spectroscopy* (Wiley Online Library)
[41] Sundaraganesan N, Ilakiamani S, Saleem H, Wojciechowski P M and Michalska D 2005 FT-Raman and FT-IR spectra, vibrational assignments and density functional studies of 5-bromo-2-nitropyridine *Spectrochimica Acta Part A: Molecular and Biomolecular Spectroscopy* **61** 2995–3001
[42] Udeshi B, Boricha H, Rajyaguru B, Gadani K, Rathod K N, Dhruv D, Kansara S B, Trivedi R K, Pandya D D, Asokan K, Solanki P S and Shah N A 2019 Electrical behavior and structure – property correlations in $La_{1-x}Pr_xMnO_3$ ($0 \leq x \leq 1$) ceramics *Ceramics International* **45** 1098–109
[43] Uncu O, Ozen B and Tokatli F 2019 Use of FTIR and UV–visible spectroscopy in determination of chemical characteristics of olive oils *Talanta* **201** 65–73
[44] Vedernikova I A 2015 Magnetic nanoparticles: Advantages of using, methods for preparation, characterization, application in pharmacy *Review Journal of Chemistry* **5** 256–80
[45] Yang J, Liu G, Zeng H and Chen L 2018 Effects of high pressure homogenization on faba bean protein aggregation in relation to solubility and interfacial properties *Food Hydrocolloids* **83** 275–86

[46] Younes H, Ravaux F, El Hadri N and Zou L 2019 Nanostructuring of pseudocapacitive $MnFe_2O_4$/Porous rGO electrodes in capacitive deionization *Electrochimica Acta* **306** 1–8
[47] Zhou X, Hu S, Wang Y, Ullah S, Hu J, Liu H and Xu B 2019 The surface adsorption, aggregate structure and antibacterial activity of Gemini quaternary ammonium surfactants with carboxylic counterions *Royal Society Open Science* **6** 190378